

# Analysis and optimisation of a rib-stiffened vaulted floor for dynamic performance

**Journal Article****Author(s):**

Wu, Hao; Liew, Andrew; Van Mele, Tom; Block, Philippe

**Publication date:**

2020-06-15

**Permanent link:**

<https://doi.org/10.3929/ethz-b-000410540>

**Rights / license:**

[Creative Commons Attribution-NonCommercial-NoDerivatives 4.0 International](#)

**Originally published in:**

Engineering Structures 213, <https://doi.org/10.1016/j.engstruct.2020.110577>

## Graphical Abstract

**Analysis and optimisation of a rib-stiffened vaulted floor for dynamic performance**

H. Wu, A. Liew, T. Van Mele, P. Block

## Highlights

### **Analysis and optimisation of a rib-stiffened vaulted floor for dynamic performance**

H. Wu, A. Liew, T. Van Mele, P. Block

- The rib-stiffened vaulted floor has high natural frequencies, low modal masses and shows general vibration sensitives.
- Qualitative and quantitative relationships among the geometric parameters, modal parameters and dynamic performance were found.
- Proper mass distribution that was found by manual and automated optimisation process accomplished considerable improvements in the dynamic performance.
- This research may provide a paradigm for future dynamic assessment and optimisation of general high frequency floors whose high frequencies are achieved by removing statically redundant mass.

# Analysis and optimisation of a rib-stiffened vaulted floor for dynamic performance

H. Wu\*, A. Liew, T. Van Mele, P. Block

*ETH Zurich, Switzerland*

---

## Abstract

There appears in the construction of modern multi-storey buildings in recent years, a prevailing trend for large bay sizes, lightweight floor systems and reduced dividing partitions. These tendencies have aroused a greater awareness of potential vibration problems when the structural floor systems are subjected to human induced activities such as footfall loading, as vibration performance may become an influential factor in the design of lightweight floor structures. A rib-stiffened vaulted floor described in this paper, can achieve sufficient structural stiffness and load-bearing capacity in an ultra-lightweight construction system. The aim of this study was to obtain a fundamental understanding of the floor's dynamic behaviour and to develop appropriate measures to improve its dynamic performance. Dynamic analyses and assessment were conducted on 180 mesh models of the floor with different combinations of geometric parameters and compared against acceleration acceptance criterion. After the parametric performance evaluations, qualitative and quantitative relationships among the geometric parameters, modal parameters and dynamic performance were found, where it was shown that most floors failed to meet the acceptance criterion. Different approaches were then taken to improve the dynamic performance of the floors, using manual distribution of additional mass or optimised relocation of constant total mass. Proper distribution of mass in targeted areas accomplished considerable improvements in the dynamic performance. This paper identifies that statically optimised low-mass floors may be particularly sensitive to footfall loading, and establishes a reliable procedure for dynamic analysis using the dynamic characteristics of a rib-stiffened vaulted floor, revealing improvements to dynamic performance and providing insight into high frequency floors.

*Keywords:* vaulted concrete floor, floor vibration, footfall loading, dynamic analysis, structural optimisation

---

## 1. Introduction

Modern building construction has been showing increasing demand for faster construction, larger bay sizes and more flexible working plan space in recent years [1]. This demand usually leads to longer spans (from 10 m-12 m) for slabs and beams (Figure 1), lightweight floor systems to reduce self-weight, and a reduced number of dividing partitions [2]. The associated reduction of flexural stiffness, lower mass per unit plan floor area, and the affect on structural damping of the floors, has initiated a greater awareness of potential floor vibration problems when the floor plates are subjected to human activities [2, 3]. Floors generate the second most frequent source of complaints from building users (the first being roofs) [4] and so special attention is needed in the design of lightweight floor systems [5].



Figure 1: An example long span composite floor system used in modern buildings (Versa-floor, developed by New Millennium Building Systems, LLC) [6].

A building with floors that show sensitivity to vibration problems may cause an apprehension for the structural safety, loss of mental concentration and an unwell feeling among the people working inside [7]. Unfortunately, once the construction of the building is complete, it can be difficult and costly to significantly improve its dynamic performance by counter-measures [8, 9], such as modifications possible by making major changes to the mass, to the structural stiffness with retro-fitting, or to the damping of the floor system by adding tuned mass dampers. Therefore, it is imperative to consider the human-induced

---

\*Corresponding author, E-mail address: wuhao@student.ethz.ch

vibration of floors at the conceptual design stage for floor systems that may show sensitivity to vibrations.

The rib-stiffened vaulted floor designed by the Block Research Group at ETH Zurich [10] conforms to the trend of lightweight floor systems in modern construction. An example of the floor element and a representative cross-section slice are shown in Figures 2 and 3. This unreinforced concrete floor element consists of a thin anti-funicular vault stiffened by a series of spandrel walls (ribs) on its extrados. The structural system is completed with tie elements or horizontal restraints, which absorb the horizontal thrusts of the shallow arching shell.



Figure 2: Exhibited physical prototype of the concrete rib-stiffened vaulted floor, supported on four corner supports and with representative steel ties.

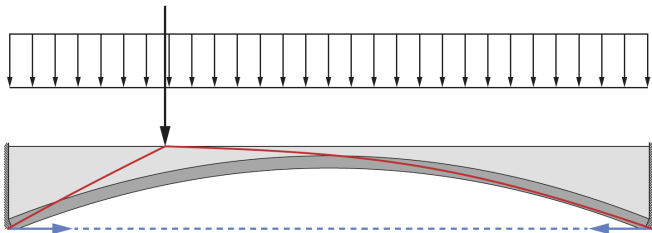


Figure 3: A cross-section diagram of a floor rib that shows the internal red thrust lines terminating at the supports and generating the blue horizontal forces, which can be taken either by ties or horizontal restraints [10].

The vaulted floor possesses some unique geometric and modal features that differentiate itself from regular concrete slabs and steel-concrete composite floors. A high stiffness can be achieved through ultra-lightweight construction, as the geometry of the vault is found through an interactive form-finding process based on Thrust Network Analysis (TNA) [11, 12, 13, 14, 15]. As a result, the vault behaves as a compression-only shell under self-weight dead loading, hence transferring a significant portion of external loads through compression in a manner that is stiffer and more efficient than through bending. Thus, the floor element is able to save up to 70% of the material weight compared to traditional solid concrete slabs, meanwhile keeping deformations lower than 1/500 of the span in the

serviceability limit state [10, 16, 17]. As a direct consequence of the floor's stiffness, it exhibits a high fundamental frequency, which can be observed in relation to the natural frequency equation of a single degree of freedom system with

$$f_n = \frac{1}{2\pi} \sqrt{\frac{k}{m}}, \quad (1)$$

where  $k$  is the stiffness and  $m$  the mass. This equation indicates that if the structure is optimised with high stiffness while mass is removed, the structure will exhibit a high natural frequency. The series of vaulted floors studied in this research paper have fundamental natural frequencies ranging from 20 Hz to 100 Hz. The cut-off frequency in standard construction differentiating low frequency floors (LFFs) and high frequency floors (HFFs) is commonly referred in engineering practice to be around 10 Hz [18]. The vaulted floor is therefore a high frequency floor, in which resonant build up does not occur and the response is a series of rapidly decaying responses following each footfall [18, 19].

Due to the structural optimisation for lower material usage, a low modal mass is to be expected, as much of the mass is removed from the mid-span region as it contributes least to either stiffness or strength. On the contrary, a considerable amount of mass is distributed to the perimeter of the floor due to the stiffening ribs and their higher depth. A solid rectangular floor has a modal mass of 25 % of the total mass (given that the mode shape is so normalised that the maximal item is 1) [20], whereas the floor under investigation here is only 1 %-7 % when the vault and ribs are of equal thickness. The vault and ribs interaction, which is not a topic for regular floor systems, plays a significant role in its dynamic behaviour.

Among excitation sources, human footfall loading is the most relevant excitation for office spaces in building floor plates [2, 21, 22]. As many factors play a role in the nature of floor vibrations, rational calculations of vibration amplitudes induced by pedestrian excitation can become complex. Consequently, empirical methods have been developed to deal with this [7]. For LFFs, since the uncomfortable vibration amplitudes are mainly caused by a coincidence of the natural frequency with the pacing frequency of footfall forces, a sufficiently high natural frequency can effectively "tune-out" a floor over the frequency range of the primary harmonic components of the walking activity, thus it protects against the likeliness of resonant behaviour. That is the principal idea of the "high tuning method" [7]. Historically, designers have used the natural frequency of the floor as the sole measure of acceptable performance [23]. In the United Kingdom, the traditional approach used to design conventional floors for serviceability criteria has been to check the primary and secondary beams independently for a minimum natural frequency of 4.0 Hz [18]. For HFFs, the "heel impact method" could be used to assess the dynamic response in the transient

phase, which consists of a person weighing 700 N raising their heels high and suddenly dropping them to the floor. The peak acceleration from this impulse is to be calculated or measured and then compared with acceptability limits applicable to the floor properties [7].

Early acceptability criteria that were based on the above methods cannot represent a realistic assessment of the vibration behaviour likely to arise in normal service [19], and so may be unacceptable. Conversely, some floors under such a design frame could be over-conservative [18]. Current European design codes do not give any clear natural frequency limit to avoid vibration problems, neither do they suggest any analysis approach for the evaluation of the dynamic performance. The vibration of concrete structures, as a serviceability limit state, is not covered in Eurocode 2 (Design of concrete structures) [24]. In Eurocode 3 (Design of steel structures) and Eurocode 4 (Design of composite steel and concrete structures), requirements for vibrations should be specified for each project and agreed with the client [25, 26]. As a result, there has been research on floor vibrations and vibration criteria. When the problem is limited to vibration perception by humans, a comprehensive review is given by [2], with the relevant standards for human perceptibility of vibration being BS6472 [27] and ISO2631 [28]. To predict the dynamic performance of floors, rather than conducting experiments and taking measurements for each design, guidelines that suggest excitation input, response assessment process and acceptability criteria are recommended. The following guidelines published by different research institutes and companies are available for this purpose: P354 by the Steel Construction Institute (SCI) [18], the Arup method [29], design guide by American Institute of Steel Construction (AISC) [30], EUR 21972 by the Technical Steel Research of European Commission (TSR) [31], EUR 24084 by the Joint Research Center of European Commission (JRC) [32], and HiVoSS guideline by the Research Fund for Coal and Steel (RFCS) [33]. The evaluation guideline P354 by the SCI is selected in this study for several reasons. Firstly, it simplifies the dynamic excitation as a series of deterministic values varying with time, rather than a probabilistic manner considering the deviation in weights and pacing frequencies of walking people (adopted by JRC and HiVoSS), which makes the analysis computationally intensive and the hidden associations between input and output somewhat unclear. Secondly, some guidelines are considered to be too conservative (the footfall input of TSR is 40% higher than that of SCI), especially when combined with a series of conservative modelling assumptions in this study. Finally, the SCI document provides users with comprehensive and important hints for modelling and implementation, it has also gained use in more practical applications than other guidelines.

Arup conducted research and compared the relative vibration performance of different forms of construction for hospital use [34]. It concluded that although the natural frequency is an important dynamic parameter, it does not

necessarily follow that a floor with a higher frequency will have a lower dynamic response. In fact, the reverse may be true if the frequency is increased by removing mass. This finding indicates the possibility that when a floor is optimised towards a statically stiff and strong structure with reduced material (usually accompanied with a high natural frequency), it may still show vibration sensitivity. Little, if any research, regarding dynamic behaviour has been performed for vaulted floors of any kind. A theoretical, experimental or empirical benchmark in terms of modal characteristics or dynamic response associated with vaulted floors has not been found by the authors. Therefore there exists a need for general high frequency floors whose geometry is achieved by removing statically redundant material, to study their dynamic performance and determine crucial parameters affecting their behaviour. This study is limited to explore the dynamic performance of the vaulted floor under single person walking excitation, as a single person walking was determined to be the most frequent source of vibration which causes a high degree of objection [35].

In pursuit of a fundamental understanding of dynamic behaviour, the following issues have been addressed in the study: 1) Section 2 develops an analysis procedure for dynamic performance, allowing fast, accurate solutions of the dynamic process; 2) Section 3 identifies key parameters that influence the dynamic performance by a parametric study, and finds qualitative and quantitative relationships among geometry, modal property and dynamic performance. Based on the above, Section 4 conducts an optimisation in two steps: 1) Sections 4.1 and 4.2 find the optimal mass and stiffness distribution under certain conditions; 2) Section 4.3 demonstrates the feasibility of attaining such mass and stiffness distribution in reality, considering fabrication constraints. Conclusions are finally presented in Section 5.

## 2. Methodology

This section presents the evaluation procedure of the floor's dynamic performance, with basic modelling assumptions given in Section 2.1, the theoretical background for solving dynamic response in Section 2.2, evaluation of vibration perception follows in Section 2.3, validation of modal superposition with finite element software in Section 2.4, and finally frequency weighting and modes selection for modal superposition presented in Section 2.5.

Figure 4 illustrates the general workflow for the evaluation of the rib-stiffened vaulted floor's dynamic performance as described in this section. The first step was to create mesh models in the CAD software Rhinoceros with different combinations of key geometric parameters. Then, these mesh models were exported into the finite element software Abaqus for a modal analysis. As a next step, modal parameters such as natural frequencies, modal masses and mode shapes from the modal analysis, were extracted to solve the response time history of the floors un-

der footfall excitation via modal superposition. Once the response from each mode was available, post-processing of the response was conducted based on the procedure presented by SCI P354 and compared with the acceptance criteria.

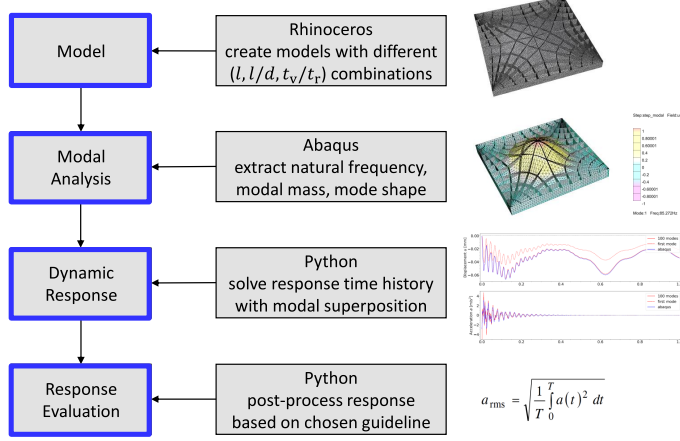


Figure 4: General workflow for the evaluation of floor dynamic performance, consisting of: 1) parametric generation of mesh models, 2) finite element modal analyses, 3) dynamic time history analysis using modal superposition, and 4) evaluation of acceleration response and comparisons to acceptance criteria.

### 2.1. Modelling

Three parameters were considered to outline the geometry of a floor for a fixed pattern (in plan) of the ribs: the span  $l$ , span to depth ratio  $l/d$ , and vault to ribs thickness ratio  $t_v/t_r$ . Some assumptions were made to reduce the complexity of the study: 1) the floors had a square form in plan, 2) the vault and ribs had constant thickness, although the vault and ribs could show different thicknesses, and 3) the highest point of the surface that runs through the middle thickness of the vault was 5 cm below the top floor level and that this did not change with the span. The parameters had the following realistic ranges for practical use as well as reasonably exaggerated values for research investigations, leading to 180 models for study:

$$\begin{aligned} l &= [5, 6, 7, 8, 9, 10] & [\text{m}], \\ l/d &= [10, 12.5, 15, 17.5, 20] & [-], \\ t_v/t_r &= [0.1, 0.5, 1, 2, 5, 10] & [-]. \end{aligned}$$

The geometry of the vault and ribs was form-found based on TNA, created with the `compas_tna` package of the opensource COMPAS framework [36]. To ensure that floors with different spans had similar ribs density (that is a similar panel size surrounded by ribs), the number of ribs in both circular and radial directions were scaled in proportion to the span, leading to a rib located every 0.5 m along the floor edges. For fair comparisons, the thickness of the vault and ribs was given in the form of a thickness ratio under the condition that the floor mass was a constant

value, no matter how the ratio varies. It has been shown experimentally that material reduction of 70 % compared to flat concrete slabs produce stiff and strong floor geometries [10][16][17], a value similar to this at a 60 % reduction was used in this research, i.e. 40 % the mass of a solid flat slab with the same plan geometry.

If the total volume of the floor  $V$ , the middle surface areas of the vault  $A_v$  and ribs  $A_r$ , and thickness ratio  $\gamma = t_v/t_r$  are given, the thickness of ribs and vault can be determined by

$$t_r = \frac{V}{\gamma A_v + A_r}, \quad (2)$$

$$t_v = \gamma t_r. \quad (3)$$

Figure 5 shows the mesh model of the floor with  $l = 5$  m and  $l/d = 15$ , with the selected mesh refinement level for an accurate finite element result based on a mesh discretisation study.

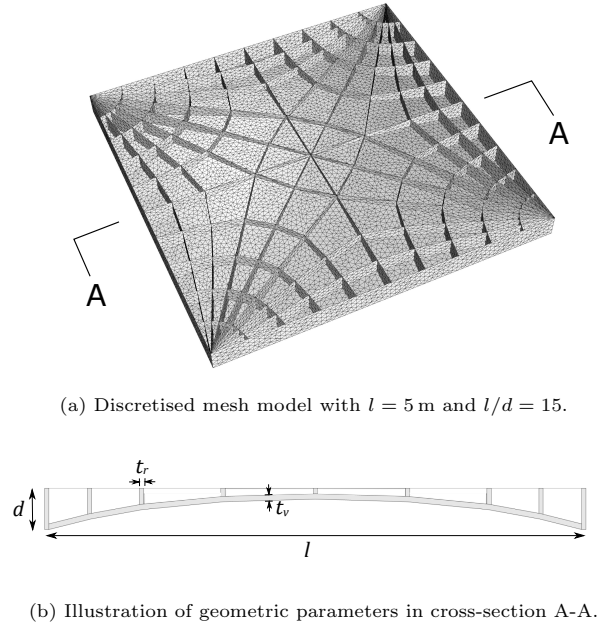


Figure 5: An example of discretised mesh mode with geometric parameters to be studied.

The floor was modelled with standard concrete material values, where the density and Poisson's ratio were set to  $2400 \text{ kg/m}^3$  and 0.2 respectively. The Young's modulus of the concrete was taken with a higher value for a dynamic process, with a dynamic Young's modulus of 38 GPa used as proposed by SCI P354 for normal weight concrete, irrespective of the actual concrete class. Linear shell finite elements (type S3 and S4 in Abaqus) were provided to represent the floor mesh in subsequent finite element models. The floor rested without constraining rotations on the four supporting edges and so have been considered as lines of pinned nodes. In footfall vibration scenarios, the expected strains are not sufficiently large enough to overcome friction [18], even though the floor may have roller boundary

conditions for static analysis. The structural frame that would support the floor element in the real construction setting was not considered as part of the modelling, both for simplicity and is also representative of its intended decoupled use. A damping ratio of 3% was assumed for fully fitted-out and furnished floors in normal office use [18]. The beneficial influence of office partitions on the stiffness and additional masses of furniture and finishing were conservatively not considered.

## 2.2. Solution of dynamic response

The excitation point and response point coincided at the mid-span of the floor to produce the maximum vibration response. Only the points that corresponded to the maximum amplitudes for each mode needed to be checked [18], and so as the first mode whose vibration shape has its peak in the middle of the span dominates the response, the footfall excitation was presumed to act at this location. Continuous footfall excitation in the same location for a long period of time is uncommon, but it is representative of the worst possible loading scenario for a given forcing function. The forcing function  $P$  varying with time  $t$  from walking activity, was assumed to be perfectly periodic and was represented by the sum of four harmonic Fourier series components based on SCI P354 as

$$P(t) = W \left[ 1 + \sum_h \alpha_h \sin(2\pi h f_p t + \beta_h) \right], \quad (4)$$

where

- $W$  is the weight of an average person, here taken as 746 N,
- $h$  is the harmonic mode number,
- $\alpha_h$  is the dynamic coefficient for mode  $h$ ,
- $f_p$  is the pacing frequency, and
- $\beta_h$  is the phase angle.

These Fourier coefficients can be extracted from Table 1, where a pace frequency of 2 Hz was adopted for this study. Figure 6 plots the footfall load–time history for one walking cycle (i.e. two pace periods), showing that the peak force value could be ca. 70% higher than the static value.

Table 1: Fourier coefficients for walking activities based on SCI P354.

Harmonic	Pace frequency	Dynamic coefficient	Phase angle
$h$	$h f_p$ (Hz)	$\alpha_h$	$\beta_h$
1	1.8 to 2.2	$0.436(h f_p - 0.95)$	0
2	3.6 to 4.4	$0.006(h f_p + 12.3)$	$-\pi/2$
3	5.4 to 6.6	$0.007(h f_p + 5.2)$	$\pi$
4	7.2 to 8.8	$0.007(h f_p + 2.0)$	$\pi/2$

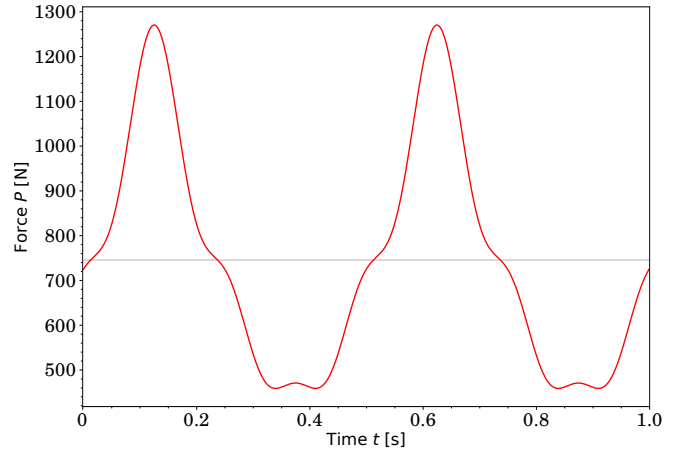


Figure 6: Footfall loading for one walking cycle (two pace periods of 0.5 s each) based on SCI P354.

The equation of motion with displacements  $\mathbf{u}$ , for a multi degree of freedom (MDOF) system with damping, is given by

$$\mathbf{m}\ddot{\mathbf{u}} + \mathbf{c}\dot{\mathbf{u}} + \mathbf{k}\mathbf{u} = \mathbf{P}, \quad (5)$$

where the square matrices  $\mathbf{m}$ ,  $\mathbf{c}$  and  $\mathbf{k}$  represent the mass, damping and stiffness of the system, and  $\mathbf{P}$  is the external loading. A direct solution of this equation set is made challenging by the coupled terms, as in normal cases the stiffness matrix  $\mathbf{k}$  and damping matrix  $\mathbf{c}$  have off-diagonal terms. The simultaneous solution of these coupled equations is generally not efficient, especially with a large number of degrees of freedom (DOF). An alternative approach is to expand the displacement vector  $\mathbf{u}$  of the MDOF system in terms of  $N$  modal contributions expressed as

$$\mathbf{u}(t) = \sum_{n=1}^N \mathbf{u}_n(t) = \sum_{n=1}^N \phi_n q_n(t), \quad (6)$$

where  $\phi_n$  is the mode shape and  $q_n(t)$  is the associated modal coordinate. Observe that the vibration of each mode is decomposed into two parts, the mode shape that characterises the vibration pattern along DOFs and stays invariant to time, the modal coordinate that represents the amplitude of vibration along time points and keeps unchanged for each DOF. Using Equation 6, the coupled Equation 5 can be transformed into a set of uncoupled equations with modal coordinates  $q_n(t)$  as the unknowns. The equation that governs the  $n^{\text{th}}$  modal coordinate  $q_n(t)$  is

$$\ddot{q}_n + 2\xi_n \omega_n \dot{q}_n + \omega_n^2 q_n = P_n(t), \quad (7)$$

where  $\xi_n$  represents the modal damping ratio,  $\omega_n$  the angular frequency, and  $P_n(t)$  the modal load.

To solve Equation 7, a modal analysis needs to be conducted as the first step for finding both the mode shape  $\phi_n$  and the angular frequency  $\omega_n$ . The generated mesh models, together with information about material, section properties, boundary conditions, and the load point, were

exported to the Abaqus finite element software package through the `compas_fea` Python package [37]. Figure 7 shows the first four unique modes from the finite element modal analysis (some modes are repeated due to symmetry).

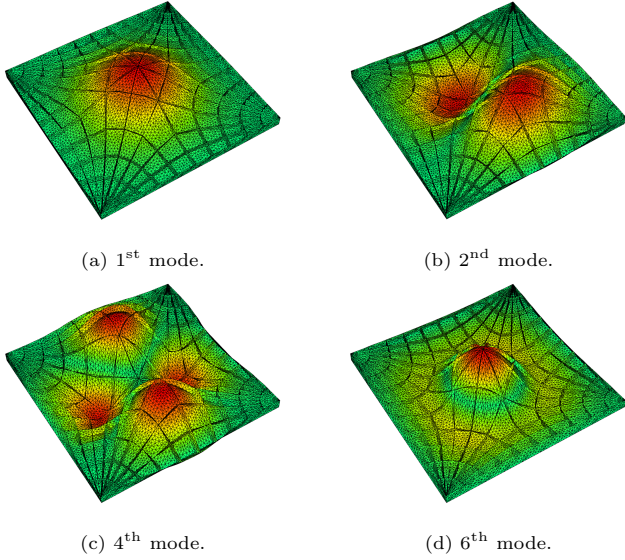


Figure 7: The first four unique modes of the floor with  $l = 5$  m,  $l/d = 20$ ,  $t_v/t_r = 1$ , as a result of a modal finite element analysis.

Once the mode shapes are available, the next step is to solve the modal coordinates  $q_n(t)$  that vary with time. In Equation 7, the modal load  $P_n(t)$  can be calculated as follows. First, express the external load  $\mathbf{P}(\mathbf{s}, t)$  acting on the MDOF system in terms of spatial distribution  $\mathbf{s}$  and time variation  $P(t)$ ,

$$\mathbf{P}(\mathbf{s}, t) = \mathbf{s}P(t), \quad (8)$$

where the spatial distribution  $\mathbf{s}$  is a vector of length equal to the number of DOFs in the system, with representative value in position whose corresponding DOF is loaded, and with 0 if not loaded. The time variation  $P(t)$  is the footfall loading expressed in Equation 4. Then calculate the modal participation factor

$$\Gamma_n = \frac{\phi_n^T \mathbf{s}}{m_n}, \quad (9)$$

where  $m_n$  denotes the modal mass. Then finally calculate the modal load by

$$P_n(t) = \Gamma_n P(t). \quad (10)$$

Once the modal load is obtained, the second order ordinary differential equation of Equation 7 can be reformed into two first order ordinary differential equations, expressed in matrix form as

$$\begin{bmatrix} \dot{q}_n \\ \dot{\dot{q}}_n \end{bmatrix} = \begin{bmatrix} 0 & 1 \\ -\omega_n^2 & -2\xi_n\omega_n \end{bmatrix} \begin{bmatrix} q_n \\ \dot{q}_n \end{bmatrix} + \begin{bmatrix} 0 \\ P_n(t) \end{bmatrix}. \quad (11)$$

This system of equations was solved with the ordinary differential equation solver `odeint` from the Python scientific library SciPy. Two initial conditions were assumed at  $t = 0$  that represent a rest state, the initial displacement  $q_n(0) = 0$  and initial velocity  $\dot{q}_n(0) = 0$ . The results of the `odeint` solver are the displacements and velocities in modal coordinates against time, and then the accelerations can be calculated by differentiating the velocities with respect to time. Once the modal coordinates  $q_n(t)$  have been solved, the total displacements can be obtained via modal superposition as expressed in Equation 6.

### 2.3. Evaluation of vibration perception

The evaluation of the dynamic performance was based on the vibration perception of humans, as characterised by the frequency weighted root-mean-square (rms) acceleration of the floor under the footfall loading, expressed by

$$a_{w,\text{rms}}(t) = \sqrt{\frac{1}{T} \int_0^T a_w^2(t) dt}, \quad (12)$$

where  $T$  is the period under consideration, here taken as  $1/f_p$ . The frequency weighted total acceleration  $a_w(t)$  was found by the summation of the acceleration responses  $a_{n,w}$  of each mode

$$a_w(t) = \sum_{n=1}^N a_{n,w}(t). \quad (13)$$

The vibration perception of humans is different with varying vibration frequencies. Humans are generally less sensitive to vibrations with very low or very high frequencies, and so the actual predicted accelerations should be weighted to reflect this. The frequency weighting function for vertical (gravity direction) vibration is  $W_b = 16/f_n$  for  $f_n > 16$  Hz based on SCI P354, which was applied to all of the studied floors. The weighted acceleration then reads as

$$a_{n,w}(t) = W_b(f_n) a_n(t), \quad (14)$$

where  $a_n(t)$  is the actual acceleration in each mode as solved by the response time history analysis.

The next step was to calculate the response factor  $R$ , which is the ratio between the weighted rms acceleration  $a_{w,\text{rms}}$  (peak value) calculated by Equation 12 and the base value  $a_{\text{base,rms}} = 5 \times 10^{-3}$  m/s<sup>2</sup>. The response factor should not exceed the recommended multiplying factors by SCI P354, which for office buildings is set as a maximal response factor of  $R = 8$ .

$$R = \frac{a_{w,\text{rms}}}{a_{\text{base,rms}}} = \frac{a_{w,\text{rms}}}{0.005}. \quad (15)$$

### 2.4. Validation of modal superposition

The theoretical background and solution procedure have been described in Section 2.2. The equation of motion in modal coordinates and the response time history via modal

superposition were solved based on Equations 6 and 7 in the Python programming language. It was necessary to compare the results from the Python model via modal superposition with those from a full time history analysis in Abaqus for calibration. An Abaqus finite element model of a floor with  $l = 5$  m,  $l/d = 20$ ,  $t_v/t_r = 1$  was examined. In the Python model, the damping ratio  $\xi = 3\%$  was defined for all modes, as it is a feature of a mode. In Abaqus, the definition of damping was executed in the material module with Rayleigh damping.

The results of the response time history analysis from the Abaqus standard solver and the Python model are compared in Figure 8. The evaluation of the rms acceleration starts from  $t = T = 0.5$  s based on Equation 12, as a whole period is needed first to average the response of the slab during a single pace. A total of 100 modes were used for the modal superposition method, and the contribution of the first mode in isolation is also shown. The comparison plot shows a very good agreement between the responses calculated by the Abaqus standard solver and modal superposition method in Python when 100 modes are used. The results from the modal superposition (in solid red line) present slightly higher values in acceleration and rms acceleration than the Abaqus analysis (blue line), suggesting a slight conservative evaluation. The plotted responses indicate a very typical transient phase, where the structure vibrates at its natural frequency immediately after the excitation and the energy dissipates quickly afterwards through damping. Then the structure moves into the steady state phase, where the vibration continues at the excitation frequency. The peak rms acceleration always appeared at the first instance, namely at 0.5 s. Figure 8 also indicates that the first mode is not sufficient to represent the displacements or accelerations adequately on its own, as higher modes whose peak appears in the middle also contribute a considerable proportion to the response.

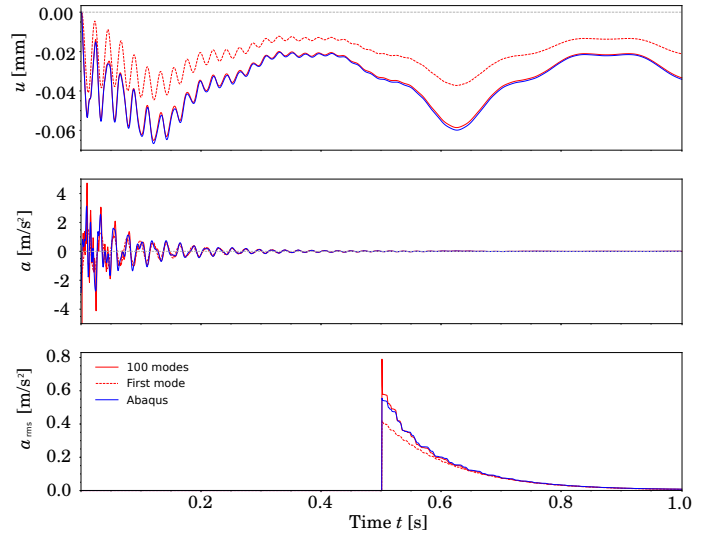


Figure 8: Comparison of dynamic responses calculated by a full time history Abaqus analysis and by a Python model with modal superposition method to the footfall loading specified by Equation 4 and presented in Figure 6.

The implementation of response time history analysis via modal superposition in Python instead of directly using existing finite element software, has some prominent advantages. Modal superposition was found to be much faster than the Abaqus standard solver for dynamics, for the floor shown in Figure 8, Abaqus took 20 times longer. In addition, it provides the possibility to access easily data for each mode, which is crucial for the post-processing of the original response, for example for frequency weighting. Besides, it gives more structural insight into the dynamic behaviour, so that the correlation between input parameters and dynamic response can be explained and checked.

### 2.5. Frequency weighting and modes

Note that for the rms acceleration subplot in Figure 8, the frequency weighting was not included. Figure 9 shows both the original and weighted rms accelerations, where it is clear that the frequency weighting plays a very important role by reducing the response by 70% (for this particular floor). It can also be seen that the response from the first mode can now represent the total response more accurately, as more than 88% of the total response is now contributed by the first mode. The frequency weighting has a peak clipping effect by filtering out the response from higher modes.

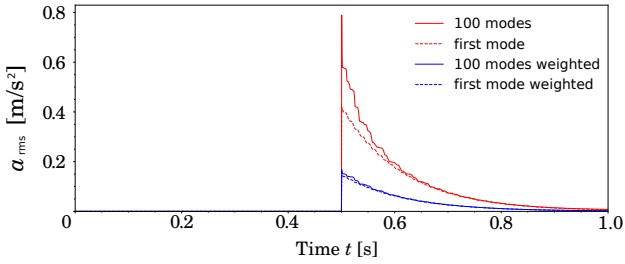


Figure 9: Original (red) and weighted (blue) rms acceleration showing the filtering effect of higher modes.

One important parameter in the solution accuracy of the modal superposition response, is to choose an adequate number of modes to combine. On the one hand, it can not be too few so that the response loses its accuracy, while on the other hand, it should not be too many so that the computation becomes heavy. An objective indicator of the actual contribution of each mode would be the modal contribution factor, which is defined as the ratio of response associated with a certain mode to the total response of all combined modes,

$$\bar{r}_n = \frac{R_n}{R}. \quad (16)$$

The calculation of contribution factors showed that the unweighted response had more contribution from modes other than the first mode, while the weighted response heavily relied on the first mode. The contribution of the first mode to the weighted response varied from 86 % to 92 % for all of the studied floor models, therefore the response from the first mode is a good indicator of the total response. Although the weighted response factor was almost unchanged after 30 modes for the floor with  $l = 5$  m,  $l/d = 20$ ,  $t_v/t_r = 1$ , 50 modes were used for the calculation of all floors for a guaranteed accurate analysis. Another reason is that this floor has a fundamental frequency of  $f_1 = 76$  Hz, which leads to a very strong frequency weighting effect, while there were also some floors with fundamental frequencies as low as 20 Hz. These lower frequency floors needed more modes for superposition, as the response from high modes could not be effectively filtered out and would contribute to the total response. Note that the required number of modes for analysis was found to be suitable to our case and needs a new evaluation for other imposed loading and structural systems.

### 3. Results

This section displays the results of the parametric dynamic analyses that were taken: Section 3.1 describes the main findings from the modal analysis, while Section 3.2 and Section 3.3 explore the influence of geometric parameters and modal parameters on dynamic performance, respectively.

#### 3.1. Modal analysis

Modal masses, natural frequencies and mode shapes were the output of the modal analyses, and reflect the dynamic characteristics of the floors. It is meaningful to observe how the input geometric parameters  $l$ ,  $l/d$ ,  $t_v/t_r$  influence these modal parameters. The modal mass reflects how much mass is effectively activated in the vibration, influenced by the total mass of the floor. The dimensionless parameter  $m_1/m$  reflects the proportion of mass (for mode one) that participates in vibration.

It was found that the correlation of  $l$  and  $l/d$  with modal mass proportion was weak, but the increase of  $t_v/t_r$  raised this parameter greatly, as seen in Figure 10. This is due to different mass and stiffness distributions in the vault and ribs. The vault has a more or less uniform mass distribution over the whole plan area, whereas the ribs have much higher mass and stiffness concentration around the floor perimeter at the support edges, allowing only a small proportion of mass in the mid-span to participate. It was found that no matter how these parameters changed, the modal mass proportion compared to the total mass reached no more than 14 %, and on occasion was found lower than 0.5 % if rib thickness dominated.

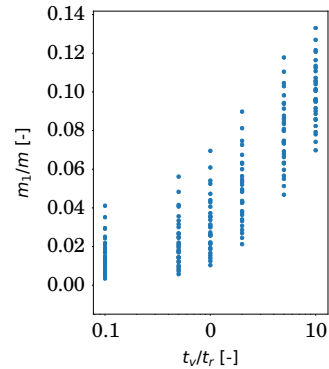


Figure 10: Plot of  $m_1/m - t_v/t_r$ , indicating that floors that had high  $t_v/t_r$  tended to have a higher modal mass proportion.

The fundamental natural frequency ( $f_1$  for mode one) is an important quantity for both low frequency as well as high frequency floors. For low frequency floors, it may be associated with resonant behaviour if the frequency is close to the pacing frequency of around 2 Hz. For high frequency floors, it is the frequency at which the floor vibrates in the transient phase. The natural frequency is also involved in the evaluation of vibration perception by the frequency weighting function. Different from the modal mass proportion, the fundamental frequency was found to be more sensitive to changes in  $l$  and  $l/d$ . Figure 11 suggests that longer and more slender floors generally show lower fundamental frequencies, although all frequencies were above 20 Hz.

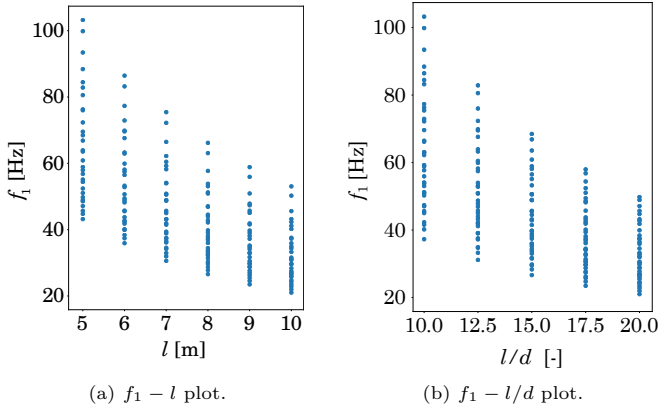


Figure 11: Plots of  $f_1-l$  and  $f_1-l/d$  plot suggest that that longer and more slender floors generally show lower fundamental frequencies.

All of the floors showed similar first six mode shapes. The ribs of the floor tend to restrict the vibration into a smaller region at the mid-span, while the vault tends to disperse the vibration to a larger region (Figure 12 is a demonstration of this). When the vault dominates, the region with large vibration amplitude expands compared to a ribs dominating floor.

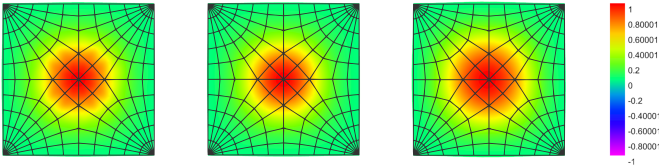


Figure 12: The first mode displacement shapes with  $t_v/t_r = 0.1, 1, 10$  from left to right, showing that when the vault dominates, the region with large vibration amplitudes expands.

### 3.2. Influence of geometric parameters

The dynamic performance of the 180 floors with different  $l, l/d, t_v/t_r$  combinations were evaluated, as characterised by the weighted response factor  $R$ . Figure 13 shows the influence of the geometric parameters on the response factor by plotting the contour lines of  $R$  against  $l/d$  and  $t_v/t_r$  for  $l = 5\text{ m}$  and  $l = 10\text{ m}$ . In both plots, the response factor  $R$  increases with  $l/d$  and decreases with  $t_v/t_r$ , which means that a slender and ribs dominated floor will have a larger value of  $R$ . This observation matches with previous conclusions associated with the modal mass and natural frequency.

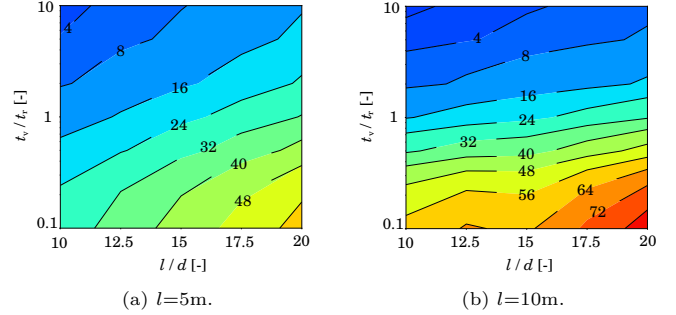


Figure 13: Response factor  $R$  contours plotted against  $l/d$  and  $t_v/t_r$  for two different spans. They indicate that higher  $l/d$  and lower  $t_v/t_r$  ratios result in a more pronounced responses. With increasing span the  $l/d$  ratio plays a less influential role.

However, two trends that differentiate the two subplots can be observed: a wider range of response factor (especially the upper bounds) and a less important role of  $l/d$  with increasing span. The former can be explained by the reduction in natural frequency caused with longer spans, that cannot be compensated by the increase in modal mass when  $t_v/t_r$  is very low. The latter may lie in the concentration of ribs on the sides in large spans. The increase in natural frequency with a lower  $l/d$  value is credited to a more fully developed arch effect. Since more mass is concentrated in ribs around the edges, the arch effect is weakened, so the  $l/d$  value cannot influence the natural frequency so well.

It is worth mentioning that for very shallow arching of the vault (large  $l/d$  value beyond the limits in the paper), the demand on the horizontal restraints, both displacement-wise and force-wise, increases rapidly, and could also lead to issues with snap-through buckling and difficulties in controlling displacements under serviceability limit state (SLS). Also, more dynamic issues are expected with very shallow floors, because the greater the horizontal movements at supports due to the failure to fulfill the high horizontal restraint demand, the less the arching action is mobilised and the greater the floor acts in bending. This bending effect will reduce the stiffness of the floor element, as the arching load take-down is a stiffer path than through flexure, leading to dynamic improvements through stiffness and frequency increases. The  $l/d$  proportions that are presented represent feasible values that have also been verified experimentally [10][16][17] and with numerical models, to engage sufficiently the arching action and not place too greater demand on the horizontal supports.

### 3.3. Influence of modal parameters

The influence of geometric parameters on the response factor is not direct, as whatever the change in geometry, it will be first reflected in the modal properties, and then transferred to dynamic performance. The relationships between geometry and modal properties has been explored in Section 3.2, and so the next step is to examine how the modal parameters influence the dynamic behaviour. As the modal parameters always relate to a certain mode,

a clear relation only exists in the modal property and the modal response resulted from it. Since the first mode dominates the contribution to the total response, the findings related to the first mode can be applied to the overall behaviour to a great extent.

Modal mass, natural frequency and mode shape are the three modal parameters that influence the response factor. Figure 14 shows the  $R_1$  (response factor for mode one) contours plotted against  $m_1$  and  $f_1$  (modal mass and natural frequency for mode one) for the different spans. The contour lines from different spans are in alignment with each other, which is no coincidence, as no matter how different the geometry of two floors may be, as long as they have the same modal property they are identical in modal space and will have the same response factor. It can be seen that a higher natural frequency and a greater modal mass will both contribute to a lower response factor, but to a different degree depending on the initial situation. The gradient of the contour lines implies that the frequency has a greater impact when the modal mass is already high, or when the frequency is still low. The modal mass plays a greater role when the floor already shows a high frequency or a low modal mass. These findings indicate that if a floor has a very low modal mass or a very high natural frequency, the most efficient way to further improve the dynamic performance is to increase the modal mass, instead of trying to further raise its natural frequency, and vice versa.

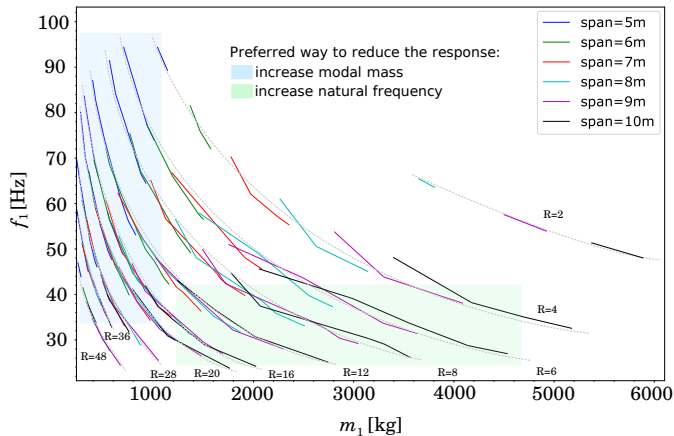


Figure 14:  $R_1$  response factor contours plotted against  $m_1$  and  $f_1$  for different spans. The  $R_1$  contours have steep gradients when  $f_1$  or  $m_1$  is very low, suggesting the most efficient direction to reduce the response further.

Figure 14 is independent from the floor geometry, this property may endow it to a new utility - as a table look-up. As long as  $m_1$  and  $f_1$  are known from a modal analysis of a floor under investigation, the response factor can be directly taken or interpolated from a plot such as this. The solution of response time history and post-processing of the data can then be skipped, thus a considerable amount of time can be saved, for example for an engineering design of a new floor geometry. This can be practical for a

quick check of the response after the simple modal analysis has been performed, or reverse, for targeting the required modal mass for a given slab span and response level (e.g. for span  $l=10$  m, response level  $R_1=8$ , a modal mass of  $m_1=2000-3000$  kg may be needed).

The quantitative relationship between the response factor and modal parameters, for the floors that have been under investigation in this research, can be expressed by the following fitted formula,

$$R_1 = \frac{C}{m_1 f_1^{1.5}}, \quad (17)$$

where  $C$  is a constant that can be obtained by a fitting process of all data points. The normalised root-mean-squared deviation between the data points and predicted values using this formula was found to be as low as 0.25 % using a  $C$  value of  $3778622 \text{ kg/s}^{1.5}$ .

#### 4. Performance optimisation

Among the studied 180 floors, only 49 of them (27 %) after analysis satisfied the acceptance criterion that the response factor  $R$  should not exceed 8, (based on the office buildings limit) under the single person excitation at mid-span. Since this left 73 % of the floor geometries having failed the check, improvement measures should be conceived. From the practical viewpoint however, this failure proportion should be treated with caution. It means that under the  $l$ ,  $l/d$ ,  $t_v/t_r$  parameter ranges that were investigated, and for the chosen mass fraction compared to a solid slab, most of these floor elements did not function well enough. If another mass fraction is given, such as 30 % mass of a solid rectangular slab with the same outer geometry instead of 40 %, some current acceptably performing floors will now fail as well.

This section will not specifically deal with the failed floors, but more generally investigate how to improve the dynamic performance of the rib-stiffened vaulted floors. This section outlines two schemes for improving dynamic performance. According to the acquired understanding of the floor's dynamic behaviour from previous sections, Section 4.1 explores improvement measures achieved through oriented trial and error. Section 4.2 introduces a surrogate model based automated optimisation procedure for distributing mass.

##### 4.1. Improvements by mass addition

Some direct improvement measurements are possible according to the analyses performed so far. For example, a thicker floor with low  $l/d$  will lead to a higher natural frequency, and more uniformly distributed mass in the vault with high  $t_v/t_r$  can greatly increase the modal mass, both changes can result in superior performance. However, sometimes the  $l/d$  ratio cannot be changed freely, for example due to construction or architectural reasons, and also the  $t_v/t_r$  ratio may not take too extreme values due

to fabrication and concrete pouring considerations. As a result, more refined and targeted improvements are necessary.

The simplified relationship between modal response and modal parameters expressed previously in Equation 17 indicated that the increase of  $m_1 f_1^{1.5}$  results in improved performance through a decrease in  $R$ . If the  $t_v/t_r$  ratio has been already raised to a reasonable value, a simultaneous increase in modal mass and natural frequency becomes very difficult. The augment in one value is sometimes only possible at the cost of a reduction in the other. If this trade off can be controlled properly, there will exist space for further improvements. Broadly speaking, there exist three scenarios with corresponding preferred solution. 1) a heavy floor already, where indeed increasing  $f_1$  has most benefit; 2) a light stiff floor, where changing  $m_1$  is most helpful; or 3) somewhere in between. As the studied slab belongs to scenario 2), changing mass is most effective. Changing  $f_1$  can be complex, as it is a function of both stiffness and mass, so requires a careful tuning of two parameters rather than one. For example adding structural mass will also make the structure stiffer, which might not change  $f_1$  as expected as it depends on  $\sqrt{k/m}$  (see Equation 1). In contrast, the increase in modal mass is easier to understand and practically realise. Figure 14 already indicated that an increase in modal mass can effectively reduce the response when the modal mass is still low and so this finding should apply to floors with short spans in particular. The modal mass for mode  $n$  is computed by,

$$m_n = \phi_n^T \mathbf{m} \phi_n. \quad (18)$$

It is intuitive that if the mass distribution represented by mass matrix  $\mathbf{m}$  conforms to the mode shape  $\phi_n$ , the matrix product will generate the highest value. Since the mode shape has its peak in the middle, the mass should also be more concentrated in the middle. One possible way to achieve this is to keep the existing constant thickness in the ribs and vault, and to add more mass where appropriate. This is effectively returning some of the mass taken away from the original structural form-finding.

Four factors may influence the effectiveness of this improvement: 1) the region where the additional mass is placed, 2) the way that this mass is added, 3) the amount of the mass increase, and 4) the geometry of the floor. Two regions to add mass have been investigated in this research, region one is located at the small innermost area (middle small), and region two includes region one and also the second inner ring of panels (middle large), as shown in Figure 15. It is assumed that the additional mass is uniformly distributed on the designated region. Two different schemes for adding mass to these two regions were tested: 1) change only the density of the regions, so that only the mass will be altered and the stiffness is kept unchanged, and 2) change the element thicknesses, which changes both the mass and stiffness of the panels at the same time. The former option represents some filling material that solely

adds the mass but without any stiffness contribution, this could be an infill material after the floor has already been cast. The latter simulates the additional mass as a structural contribution that functions together with the original ribs and vault structure, meaning this mass must be cast with the original concrete or mechanically connected to it. Mass increases as a percentage of the original mass were tested from 5% to 30%. Only floors of 5m span with the following geometric parameters have been evaluated:  $l/d = [10, 15, 20]$ ,  $t_v/t_r = [0.1, 1, 10]$ .

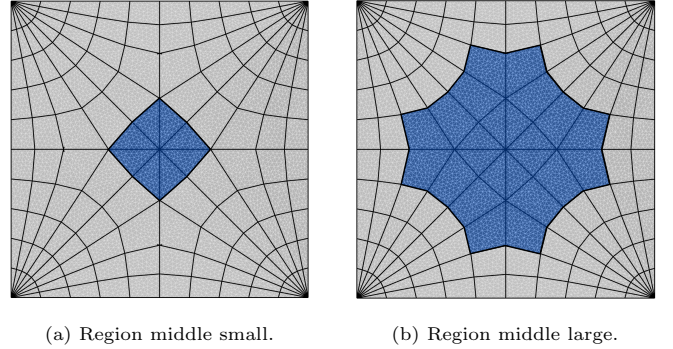


Figure 15: Two regions in the middle of the floor selected for additional mass placement. Middle small includes only the most inner area, while middle large also encompasses the second inner ring.

Figures 16 and 17 show the normalised optimal to initial  $m_1, f_1, R_1$  values of the new floors with the mass additions via density change (infill material), plotted against the relative mass increases in percent. The figures indicate that a mass addition scheme that does not modify structural stiffness, can lead to a considerable increase in the modal mass, but also results in a significant drop in the natural frequency. Take for instance the floor with  $l/d = 15$ ,  $t_v/t_r = 1$  and mass increase of 10%, where a 91% and 47% increase in the modal mass were gained for region small and region large respectively, accompanied by a 37% and 19% reduction in the natural frequency. This actually gave a rise of 6% and a drop of 6% in the response factor  $R_1$  for the two regions respectively. Other data points for region middle small (Figure 16) show either a slight improvement in  $R$  or again a deterioration in dynamic performance. The improvements for region middle large (Figure 17) are significantly better than the smaller region, with reductions in  $R$  of up to 50% and generally around 10-20%.

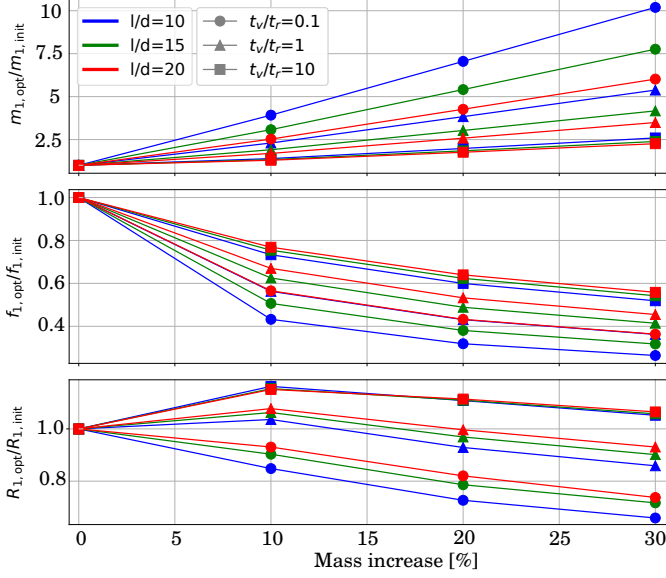


Figure 16: Normalised  $m_1, f_1, R_1$  of optimised floors in relation to mass increase (span=5m, density change, region middle small).

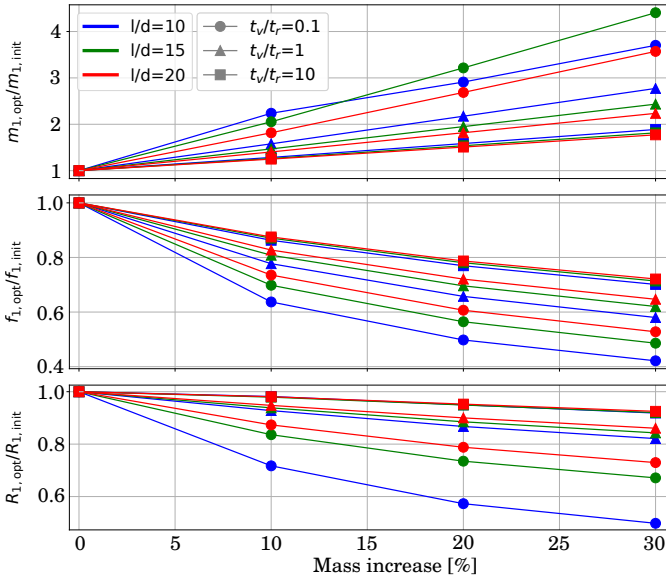


Figure 17: Normalised  $m_1, f_1, R_1$  of optimised floors in relation to mass increase (span=5m, density change, region middle large).

Figures 18 and 19 also plot the normalised  $m_1, f_1, R_1$  values of new mass added floors, yet with the mass additions via thickness change, representing additional structural mass (not infill material). The figures indicate that the mass addition scheme that also affects structural stiffness, can greatly raise the modal mass and also leads to a controlled reduction in the natural frequency. As a consequence, the improvements to the response factor  $R_1$  are considerable. For the floor with  $l/d = 15, t_v/t_r = 1$  and mass increase of 10 %, the increase in modal mass of 272 % and 107 %, although partially compensated by a 15 % and 3 % reduction in natural frequency, still led to strong de-

creases in the response factor  $R_1$  by 66 % and 49 % for region small and region large, respectively. The shape of the normalised response factor curve shows consistent performance improvements with additional mass increases, with the 5 % and 10 % mass increases producing the biggest improvements and 20 % on-wards providing less benefit. The mass addition in region small generates more pronounced response reductions than in region large. The mass addition in region large needs less thickness increase to achieve the same mass raise due to the larger area that is thickened.

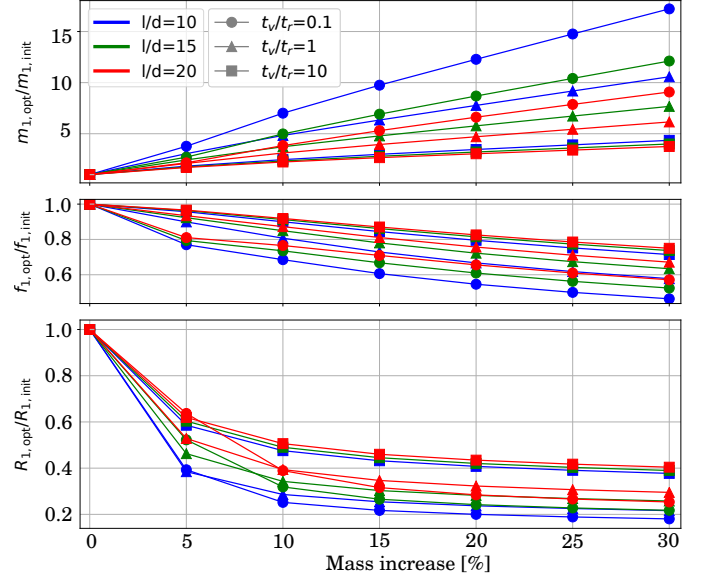


Figure 18: Normalised  $m_1, f_1, R_1$  of optimised floors in relation to mass increase (span=5 m, thickness change, region middle small).

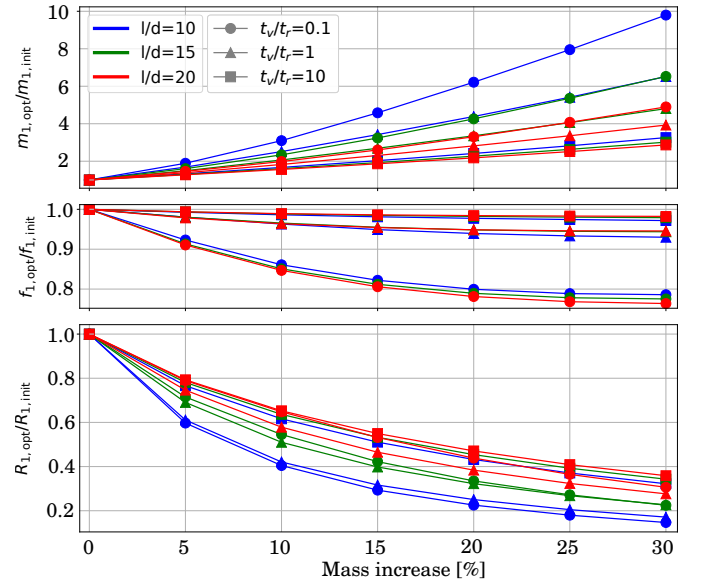


Figure 19: Normalised  $m_1, f_1, R_1$  of optimised floors in relation to mass increase (span=5 m, thickness change, region middle large).

#### 4.2. Surrogate model optimisation

The results presented so far, including the improvements by mass addition in Section 4.1, are based on floor models with uniform thickness in both the ribs and vault. It is expected that a an improved floor performance under a constant mass constraint will not necessarily have a constant thickness distribution everywhere in the vault or ribs.

To optimise the floor further with potentially non-uniform thicknesses, the dimension of the model has to be raised. When  $l$  and  $l/d$  are kept constant, the previous model has only one dimension for the given rib pattern, that is the thickness ratio of the vault and ribs  $t_v/t_r$ . To extend upon this, the floor panel areas were assigned to 41 groups, where each group could have a different thickness from others. To reduce the computational cost, only one quarter of the floor was modelled, as shown in Figure 20 using two boundary condition surfaces. To capture the mode shapes that are symmetric about both the  $x$  and  $y$  axes, the DOFs on the boundary surface  $x$  should not move along the  $x$  axis, and the rotation around  $y$  axis should be fixed, while for boundary surface  $y$ , movement along the  $y$  axis and rotation around  $x$  should be constrained. In addition, the rib thicknesses at the boundary surfaces should be halved, as they are now shared by neighbouring quarters. Natural frequencies and modal masses of the one quarter model were found to match well with the symmetric modes of the original full model.

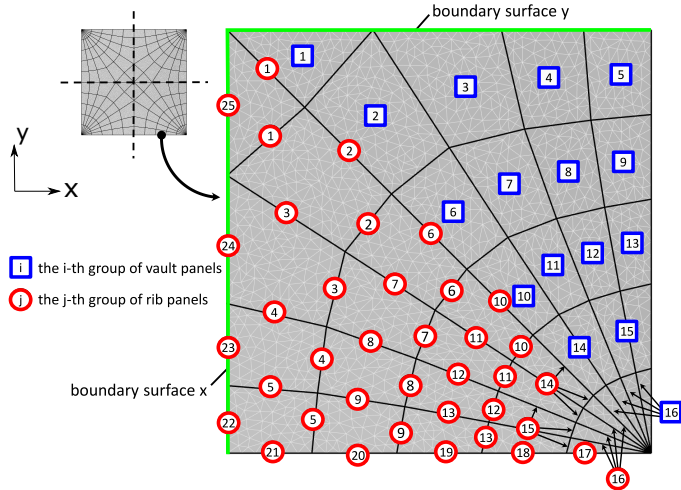


Figure 20: One-quarter model of the floor with  $l = 5$  m and  $l/d = 10$ , divided into 16 vault panel groups and 25 rib panel groups. The numbering is symmetric about the diagonal ribs and labelled only on one side for simplicity.

For such a complex model with 41 thickness dimensions, the optimisation procedure needs to be considered carefully. The Differential Evolution (DE) [38] implementation on the COMPAS framework was used in this research, which has successfully been used on other minimisation problems [39] [40]. The key solver parameters used were the Differential Evolution parameter  $F = 0.8$ , and

the cross-over ratio parameter  $CR=0.5$ , tasked with the objective of minimising the response factor  $R$  by using the thicknesses as variables. Still, the DE optimisation was found to be very time-consuming when it was applied to the full model that involved the modal analysis and solution of response time history in each evaluation of the objective function. This is because the objective function evaluation takes of the order of a few minutes, and would need evaluating many thousands of times in the  $R$  minimisation process. To accelerate the optimisation process, the DE algorithm was paired with a surrogate model that could reflect the essence of the real model but take much less time to evaluate.

A Polynomial Chaos Expansion (PCE) surrogate model [41, 42] and DE optimisation was found to be a very efficient pairing when the high complexity of the model and the low computational effort were considered. Less than 90 minutes were needed to run the experimental designs and build the PCE model, and 50000 evaluations of the PCE model for one evolutionary optimisation took only 30 seconds. The concept of optimisation through a surrogate model is shown in Figure 21. To train the surrogate model, a certain number of evaluations of the full model (with lengthy modal analysis) was necessary. Using the real (geometric input, response factor output) data sets from these evaluations, parameters that defined the surrogate model could be determined. The evolutionary optimisation was then applied to the surrogate model so that it skipped the intermediate steps and directly mapped the geometric input to the response factor output. The objective of the optimisation algorithm was to minimise the first mode response factor  $R_1$  of the surrogate model. Because the optimised input was sometimes not within the input samples that were used to train the surrogate model, the prediction from it could be biased. The values predicted by the surrogate model usually showed the trend, but not necessarily the exact numbers. Once the optimisation was finished, the input of the optimised surrogate model was used in the full model to recalculate the actual response factor.

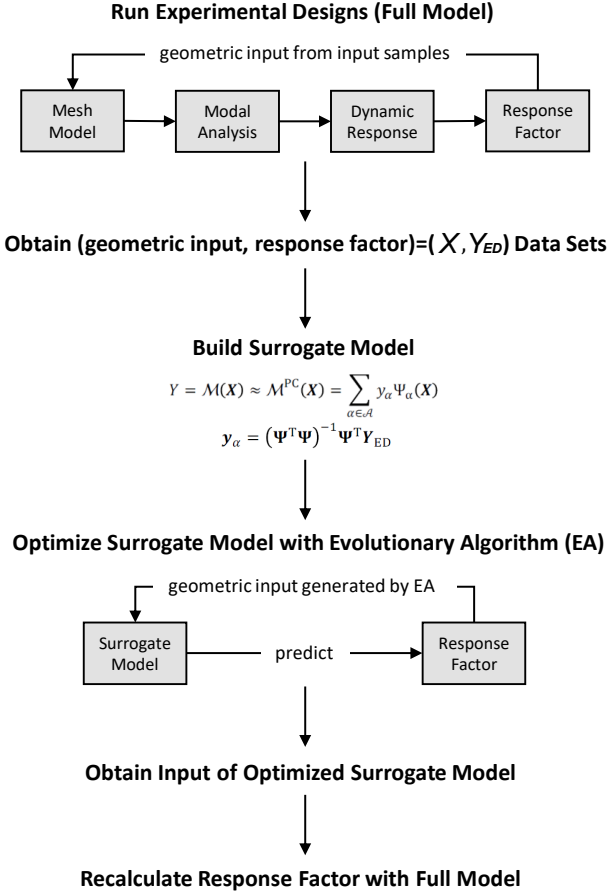


Figure 21: Flow chart of the utilised surrogate model based Differential Evolution optimisation process.

The surrogate model in this research has been assembled using a PCE model. To approximate the real model  $\mathcal{M}(\mathbf{X})$ , a surrogate truncated PCE model is built

$$Y = \mathcal{M}(\mathbf{X}) \approx \mathcal{M}^{\text{PC}}(\mathbf{X}) = \sum_{\alpha \in \mathcal{A}} y_{\alpha} \Psi_{\alpha}(\mathbf{X}). \quad (19)$$

The task is then to develop a set of appropriate polynomial basis  $\Psi_{\alpha}$  and search for corresponding coefficients  $y_{\alpha}$ . Free polynomial bases (instead of orthogonal ones for classical PCE) were implemented here for the evaluation. For a model with dimension  $M$ , the multivariate polynomial associated with certain degree indices  $\alpha = \{\alpha_1, \dots, \alpha_M\}$  is

$$\Psi_{\alpha}(\mathbf{x}) = \prod_{i=1}^M \Psi_{\alpha_i}^{(i)}(x_i), \quad (20)$$

where  $\Psi_{\alpha_i}^{(i)}(x_i)$  is the univariate polynomial of degree  $\alpha_i$  in form

$$\Psi_{\alpha_i}^{(i)}(x_i) = x_i^{\alpha_i}. \quad (21)$$

When the input  $\mathbf{X}_{\text{ED}}$  and output  $\mathbf{Y}_{\text{ED}}$  for experimental designs are available, the polynomial coefficients can be obtained via least-square minimisation

$$\mathbf{y}_{\alpha} = (\Psi^{\text{T}} \Psi)^{-1} \Psi^{\text{T}} \mathbf{Y}_{\text{ED}}, \quad (22)$$

where  $\Psi$  matrix is assembled by

$$\Psi = \Psi_{ij}(\mathbf{X}_{\text{ED}}) = \Psi_j(\mathbf{X}_{\text{ED}}^{(i)}) = \begin{pmatrix} \Psi_1(x^{(1)}) & \dots & \Psi_P(x^{(1)}) \\ \vdots & \ddots & \vdots \\ \Psi_1(x^{(n)}) & \dots & \Psi_P(x^{(n)}) \end{pmatrix}. \quad (23)$$

When the PCE has been built, meaning that the coefficients are already known, predictions can be made by

$$\mathbf{Y}_{\text{pred}} = \mathcal{M}^{\text{PC}}(\mathbf{X}) = \sum_{\alpha \in \mathcal{A}} y_{\alpha} \Psi_{\alpha}(\mathbf{X}) = \Psi \mathbf{y}_{\alpha}, \quad (24)$$

where  $\mathbf{X}$  is the thickness sets of a floor whose responses are to be predicted.

For our model with dimensions  $M = 41$ , only the first degree polynomial was used with an over-sampling rate  $k = 2$  to avoid over-fitting, and so the full model needed to be evaluated  $n = 84$  times, which was easily affordable. The thickness ratio between the thickest element and the thinnest, could be given to the DE solver as the upper bound on each dimension, while the lower bound was always set to 1. This controlled the range of thickness values returned from the optimisation process. Additionally, it was important to set a mass constraint in the solver, so that each optimisation was for a floor where the mass was being redistributed spatially, and not added or subtracted. Figure 22 shows the results from the optimised mass distributions via the PCE surrogate model based evolutionary optimisation, with different maximal thickness ratios bounds. On these subplots the darker the colour, the thicker the panels, with blue areas those that are particularly thicker. It can be seen that only boundary thickness values corresponding to certain allowable thickness ratio remain after the optimisation. The higher the allowable thickness ratio, the more freedom the mass has to concentrate on where it needs to, in order to minimise the response factor. The optimised figures with  $t_{\text{max}}/t_{\text{min}} \geq 6$  converge and remained unchanged, showing no further sensitivity.

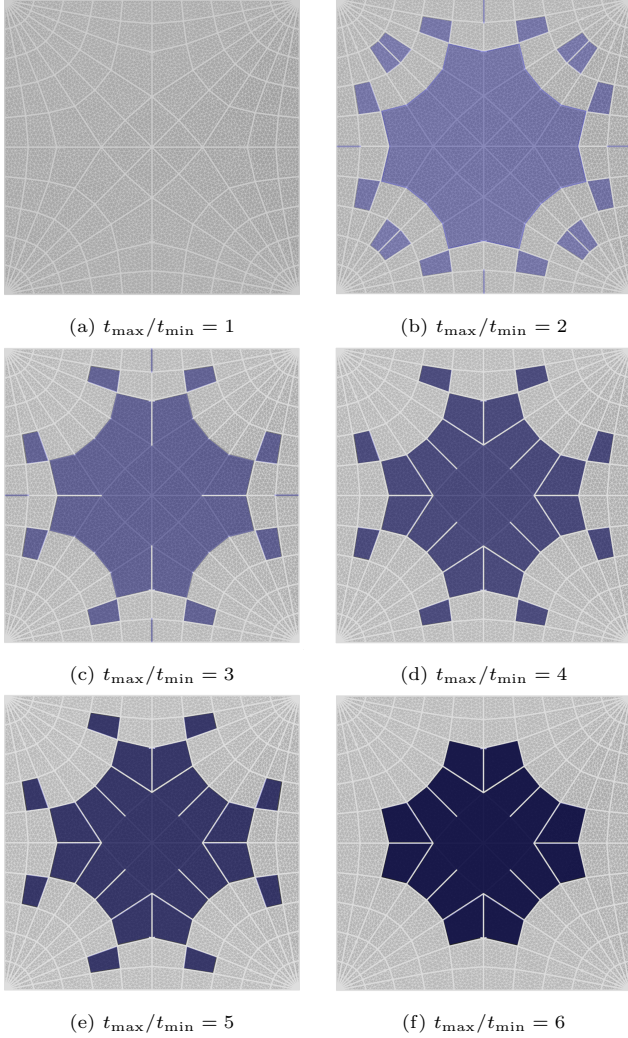


Figure 22: Optimised mass distribution of the floor with  $l = 5$  m and  $l/d = 10$ , via the PCE surrogate model and DE optimisation, for different allowable thickness ratios. The optimisation objective was minimising the first mode response factor  $R_1$ .

The dynamic performance of the initial floors that had uniform thickness in the vault and ribs (in Section 3), is compared in Figure 23 with the PCE model optimised floors with different thicknesses in each group. The response reduction (RR) shown by the blue line is calculated by

$$RR = \frac{R_{1,init} - R_{1,opt}}{R_{1,init}}. \quad (25)$$

Figure 23 shows how the response factors change in relation to allowable thickness ratios and demonstrates that a considerable reduction of up to nearly 45 % in the response has been achieved in the optimised floors. Note that these improvements are not through adding additional mass, but simply relocating it to regions that improve the dynamic performance. Combined with the previous findings in Section 4.1, we can see that having more mass situated in selected regions at the centre of the floor is where we should focus our engineering efforts.

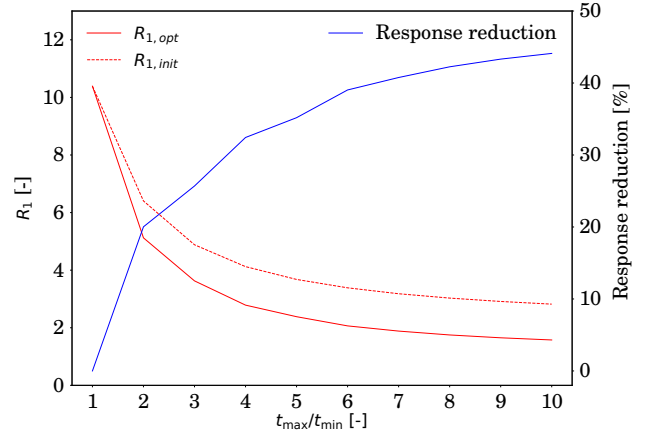


Figure 23: First mode response factors of initial floor  $R_{1,init}$  (uniform thickness in vault and ribs) and PCE model based optimised floor  $R_{1,opt}$  in relation to allowable thickness ratios, showing considerable reductions in response for the optimised floors.

### 4.3. Recommended improvements

Based on the optimised mass distribution in Figure 22, the darker thicker areas for when  $t_{max}/t_{min} \geq 6$  is exactly the selected region middle large in Figure 15 for a higher modal mass through thickness change. Both the intuitive improvements by mass addition and the more sophisticated optimisation under constant mass, indicate that thicker vault panels in the mid-span region will lead to improved dynamic performance. For the 5 m span vaulted floor case, it is recommended to thicken the vault in the larger region arrangement rather than the smaller region, as: 1) a considerable reduction in response factor can still be achieved, 50 % is achievable by adding 10 % mass and 30 %–40 % by relocating mass, 2) it creates a larger area where the footfall loading can be captured and the dynamic response alleviated, rather than just directly at the middle, 3) it is easier for fabrication to add mass over a larger area during concrete casting than locating all additional mass at a concentrated point. Figure 24 illustrates one possible improvement scheme by casting additional structural concrete of roughly uniform thickness in the larger middle region. Note that the shaded separation of the main structure and the additional structural mass in the figure is merely for illustration, they should be cast together monolithically. Adding additional mass rather than redistributing it, allows the static and dynamic designs to be performed more independently. Ideally the floor's dynamic performance will be evaluated at a time before the fabrication of the concrete formwork has taken place, as the structural changes must be integrated before the concrete has been poured monolithically. The required adjustments to the formwork design for mass addition would then be for the filling of some central panels in-between ribs, it might be more economical to fill panels to the top level rather than creating more complex formwork to fill them part way.

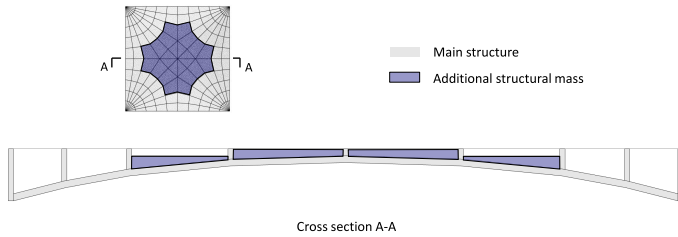


Figure 24: Recommended improvement measure that utilises the casting of additional structural concrete in the larger middle region. The main structure and additional structural mass should be cast monolithically, they are shown here separately for clarity.

By adopting this recommended improvement measure with the floor with  $l = 5$  m,  $l/d = 15$ ,  $t_v/t_r = 1$  for example, 15% mass increase is needed to reduce the response factor  $R_1$  from 19.0 to 7.5 (a 60% decrease) to meet the acceptance criterion. In this case, the total mass of the improved vaulted floor accounts for 46% ( $40\% \times 1.15$ ) of the mass of a solid slab with the same plan geometry. We can see that the extra mass for improving the dynamic performance is not a large addition, and the necessary amount can be further reduced by raising the  $t_v/t_r$  value in the initial design.

## 5. Conclusions

This study addressed the dynamic performance of rib-stiffened vaulted floors under single person footfall excitation. The fundamental dynamic behaviour of the floors differs from traditional floor systems, due to the high natural frequency deriving from stiff shallow arching action, and a low modal mass as a result of its material weight savings. As a consequence, it was found that the floors' dynamic response could be problematic, as the low modal mass could not be compensated by the high natural frequency.

Qualitative and quantitative relationships among the geometric parameters, modal parameters and dynamic performance were found, to ascertain the parameters' influence on the modal properties and the response factor. For the modal mass, the vault to ribs thickness ratio had the greatest relevance, while for the natural frequency the span and span to depth ratio had similar significance. A higher vault to thickness ratio and a lower span to depth ratio can lead to a lower response factor by increasing the modal mass and raising the natural frequency, respectively. It was also determined that the response factor attributed to the first mode dominated the total response and could be expressed in a simple equation form.

Since more than 70% of the studied floors failed the acceptance criterion, two improvement methods were investigated: by adding mass to the middle region and by an automated optimisation under constant mass. The first approach increased the modal mass by locally changing the density or structural thickness of panels in the mid-span region of the floor. Density change represented

the effect of adding a filling material, but this did not function well due to the considerable simultaneous drop in natural frequency. Thickness changes added structural mass and stiffness to the floor, and this measure very effectively reduced the dynamic response. The second approach used a surrogate model in an evolutionary optimisation method, in pursuit of the optimal mass distribution with constant mass. A first degree PCE model succeeded in greatly improving the dynamic performance while keeping the computational cost low. The results from both methods showed that a simple and effective improvement measure is to cast additional structural concrete in the middle region.

This was a preliminary study addressing the dynamic behaviour and unique characteristics of the rib-stiffened vaulted floor. Future work can focus on additional important engineering parameters, such as the effect of edge boundary conditions, relationship with supporting beams, different floor plan shapes and also rib patterns/topology. Investigations could also consider how to influence the dynamic response via modifying the natural frequency, rather than the current focus of adding additional mass (which reduces the natural frequency).

## Acknowledgements

The authors wish to sincerely acknowledge the assistance of Dr. Tomás Méndez Echenagucia (BRG) in the form-finding of the floor models, the help provided by Prof. Dr. Bozidar Stojadinovic and Dr. Marco Broccardo (ETH Zurich) in the dynamic analysis formulation, and the suggestions given by Prof. Dr. Bruno Sudret and Dr. Maliki Moustapha (ETH Zurich) in the surrogate modelling.

## References

- [1] Middleton, C. J. and Brownjohn, J. M. W. Response of high frequency floors: A literature review. *Engineering Structures*, 32(2):337–352, 2010.
- [2] Pavic, A. and Reynolds, P. Vibration serviceability of long-span concrete building floors. part 1: Review of background information. *Shock and Vibration Digest*, 34(3):191–211, 2002.
- [3] Bachmann, H. and Ammann, W. *Vibrations in structures: induced by man and machines*, volume 3. IABSE, 1987.
- [4] Garber, G. *Design and construction of concrete floors*. CRC Press, 2006.
- [5] Smith, I. and Chui, Y. H. Design of lightweight wooden floors to avoid human discomfort. *Canadian Journal of Civil Engineering*, 15(2):254–262, 1988.
- [6] New Millennium Building Systems, LLC. Versa-floor, long-span composite floor systems. <https://www.newmill.com/pdfs/Versa-Floor-systems.pdf>, 2016. Accessed: 2019-04.
- [7] Bachmann, H., Ammann, W. J., Deischl, F., Eisenmann, J., Floegl, I., Hirsch, G. H., Klein, G. K., Lande, G. J., Mahrenholtz, O., Natke, H. G., et al. *Vibration problems in structures: practical guidelines*. Birkhäuser, 2012.
- [8] Ellingwood, B. Structural serviceability review and standard implementation. In *Building an International Community of Structural Engineers*, pages 436–443. ASCE, 1996.
- [9] Research Fund for Coal and Steel. Vibration design of floors. background document., 2007.

- [10] Liew, A., López López, D., Van Mele, T., and Block, P. Design, fabrication and testing of a prototype, thin-vaulted, unreinforced concrete floor. *Engineering Structures*, 137:323–335, 2017.
- [11] Block, P. and Ochsendorf, J. Thrust Network Analysis: A new methodology for three-dimensional equilibrium. *Journal of the International Association for Shell and Spatial Structures*, 48(3):167–173, 2007.
- [12] Block, P. *Thrust network analysis: Exploring three-dimensional equilibrium*. PhD thesis, Massachusetts Institute of Technology, 2009.
- [13] O’Dwyer, D. W. Funicular analysis of masonry vaults. *Computers and Structures*, 73:187–197, 1999.
- [14] Fraternali, F. A thrust network approach to the equilibrium problem of unreinforced masonry vaults via polyhedral stress functions. *Mechanics Research Communications*, 37:198–204, 2010.
- [15] Marmo, F. and Rosati, L. Reformulation and extension of the thrust network analysis. *Computers and Structures*, 182:104–118, 2017.
- [16] López López, D., Veenendaal, D., Akbarzadeh, M., and Block, P. Prototype of an ultra-thin, concrete vaulted floor system. In *Proceedings of IASS Annual Symposia*, volume 2014, pages 1–8. International Association for Shell and Spatial Structures (IASS), 2014.
- [17] Rippmann, M., Liew, A., Van Mele, T., and Block, P. Design, fabrication and testing of discrete 3d sand-printed floor prototypes. *Materials Today Communications*, 15:254–259, 2018.
- [18] Smith, A. L., Hicks, S. J., and Devine, P. J. *Design of floors for vibration: A new approach*. Steel Construction Institute Ascot, Berkshire, UK, 2007.
- [19] Willford, M., Young, P., and Field, C. Predicting footfall-induced vibration: Part 1. *Proceedings of the Institution of Civil Engineers-Structures and Buildings*, 160(2):65–72, 2007.
- [20] Howard, C. Q. Modal mass of clamped beams and clamped plates. *Journal of sound and vibration*, 301(1-2):410–414, 2007.
- [21] Chik, T. N. T., Yabi, S., Yusoff, N. A., and Ghazali, M. I. Analysis of the effect of vibration from footfalls on office building. In *CIEC 2014*, pages 3–15. Springer, 2015.
- [22] Younis, A., Avci, O., Hussein, M., Davis, B., and Reynolds, P. Dynamic forces induced by a single pedestrian: A literature review. *Applied Mechanics Reviews*, 69(2):020802, 2017.
- [23] European Committee for Standardization. *Eurocode 3: Design of steel structures*. CEN, 1992.
- [24] European Committee for Standardization. *Eurocode 2: Design of concrete structures*. CEN, 2004.
- [25] European Committee for Standardization. *Eurocode 3: Design of steel structures*. CEN, 2005.
- [26] European Committee for Standardization. *Eurocode 4: Design of composite steel and concrete structures*. CEN, 2004.
- [27] British Standards Institution. *BS 6472: Guide to evaluation of human exposure to vibration in buildings (1 Hz to 80 Hz)*. British Standards Institution, 1992.
- [28] International Organization for Standardization. Mechanical vibration and shock-evaluation of human exposure to whole-body vibration—part 2: vibrations in buildings (1 to 80 hz). *International Standard ISO*, 2003.
- [29] Willford, M. R. and Young, P. *A design guide for footfall induced vibration of structures*. Concrete Society for The Concrete Centre, 2006.
- [30] Murray, T. M., Allen, D. E., and Ungar, E. E. Steel design guide series 11: Floor vibrations due to human activity. *American Institute of Steel Construction, Chicago*, 1997.
- [31] Sedlacek, G., Heinemeyer, C., Butz, C., Veiling, B., Waarts, P., Van Duin, F., Hicks, S., Devine, P., and Demarco, T. Generalisation of criteria for floor vibrations for industrial, office, residential and public building and gymnastic halls. *EUR*, (21972):1–343, 2006.
- [32] Feldmann, M., Heinemeyer, C., Butz, C., Caetano, E., Cunha, A., Galanti, F., Goldack, A., Hechler, O., Hicks, S., Keil, A., et al. Design of floor structures for human induced vibrations. *JRC-ECCS joint report*, 2009.
- [33] Feldmann, M., Heinemeyer, C., Lukic, M., et al. Human-induced vibration of steel structures (Hivoss). *Office for Official Publications of the European Communities, Luxembourg*, 2010.
- [34] Arup. Hospital floor vibration study, comparison of possible hospital floor structures with respect to NHS vibration criteria. *London: Ove Arup & Partners Ltd*, 2004.
- [35] Polensek, A. et al. Human response to vibration of wood-joint floor systems. *Wood Science*, 3(2):111–9, 1970.
- [36] Van Mele, T., Liew, A., Méndez Echenagucia, T., Rippmann, M., et al. Compas: A framework for computational research in architecture and structures, 2017.
- [37] Liew, A. and Méndez Echenagucia, T. compas\_fea: A finite element analysis package for python, 2018.
- [38] Storn, R. and Price, K. Differential Evolution - A simple and efficient heuristic for global optimization over continuous spaces. *Journal of Global Optimization*, 11(4):341–359, 1997.
- [39] Liew, A., Pagonakis, D., Van Mele, T., and Block, P. Load-path optimisation of funicular networks. *Meccanica*, 53(1):279–294, 2018.
- [40] Liew, A., Maia Avelino, R., Moosavi, V., Van Mele, T., and Block, P. Optimising the load path of compression-only thrust networks through independent sets. *Structural and Multidisciplinary Optimization*, 2019.
- [41] Liu, Z., Lesselier, D., Sudret, B., and Wiart, J. Surrogate modeling based on resampled polynomial chaos expansions. *arXiv preprint arXiv:1810.09116*, 2018.
- [42] Gratiot, L. L., Marelli, S., and Sudret, B. Metamodel-based sensitivity analysis: polynomial chaos expansions and gaussian processes. *Handbook of Uncertainty Quantification*, pages 1–37, 2016.